銅金合金奈米粒子之抗氧化性質及其在導電應用之研究
Oxidation resistance of Cu_xAu_{1-x} alloyed nanoparticles and its electrical conductive applications

計畫編號：96-2218-E-009-013-
執行期限：2007 年 8 月 1 日 至 2008 年 7 月 31 日
主持人：陳軍華 助理教授 (交通大學材料系)
計畫參與人員：賴相宇・張嘉倫・陳建穎

Abstract

Oxidation of Cu-Au alloy nanoparticles (10 and 40 at. % Au; ~17 nm in mean size) by exposure of 700 Torr dry air at 298 K has been investigated by means of in-situ x-ray diffraction (XRD) and ex-situ x-ray photoelectron spectroscopy (XPS). An Au-rich dealloyed phase was formed during the air exposure indicating the selective oxidation of the Cu component. The exposure time dependent oxidation and dealloying processes were recorded from the variation of the overlapped diffraction peaks of the oxide and dealloy phases. According to the kinetics analysis, a protective oxidation behavior appeared in the specimen of 10 at. % Au, whereas a non-protective oxidation showed in that of 40 at. % Au. The XPS analysis showed the existence of Cu_2O and $Cu(OH)_2$ phases in the specimen of 10 at. % Au. Nevertheless, CuO and $Cu(OH)_2$ phases were the main oxides in the specimen of 40 at. % Au.

Keywords: oxidation, dealloy, Cu-Au, nanoparticle, Cu_2O, CuO, $Cu(OH)_2$

摘要

本研究利用氣相冷凝法生成表面潔淨之 Cu-Au 合金奈米粒子(10 及 40 at. % Au; 平均粒徑~17 nm)，並於試片製備完成後，於不同的氧分壓與基板溫度控制之下，同時進行臨場 XRD 觀測，藉以了解 Cu-Au 奈米粒子之氧化動力學。臨場氧化觀測後之試片並進行 XPS 以及 HREM 檢測藉以了解 Cu-Au 合金奈米粒子在選擇性氧化之狀態下，所生成之 Cu 氧化物種類以及去合金化狀態。從 XRD 結果發現，Cu-10 at. % Au 呈現保護性氧化行為(~direct log)，亦即氧化速度隨著氧化時間的增加，而漸趨減緩，相反地，Cu-40 at. % Au 呈現非保護性氧化行為(~cubic)，亦即氧化速度隨著氧化時間的增加，並無減緩之傾向。從 XPS 結果發現，Cu-10 at. % Au 之 Cu 氧化相以 Cu_2O 與 $Cu(OH)_2$ 為主，而 Cu-40 at. % Au 之 Cu 氧化相以 CuO 與 $Cu(OH)_2$ 為主。

關鍵詞： 氧化、去合金化、銅金合金、奈米粒子、Cu_2O、CuO、$Cu(OH)_2$

Introduction

Copper electrodes and inter-connectors fabricated by deposition or print methods have been widely used in the integrated circuit devices because Cu has low electrical resistivity, low cost and high electron migration resistance. With the trend of nano-scaled and flexible devices, nano-printing techniques become one of few methods to meet these new purposes. Copper nanoparticles which have been synthesized with different methods show great potential for the nano-ink applications. However, oxidation is always the problem regardless of Cu bulk/film or nanoparticles. According to our previous studies, pure Cu nanoparticles oxidized with an extreme high speed when they just exposed to air. In addition, the oxidation kinetics drastically changes with the ambient temperature.

Add of second noble metal, e.g. Au and Pt, is expected to improve the oxidation resistance of Cu nanoparticles. Oxidation of Cu and its alloyed nanoparticles is of great importance for both theoretical and practical purposes. Till now very little is known about the oxidation in nano-scale Cu and its alloys although that in bulk cases has been

investigated for a long time. Further research is therefore needed. In this presentation, we report the quantitative analysis results of the compositional dependent oxidation of Cu-Au alloy nanoparticles. This work can provide fundamental understanding of Cu-Au nano-particular system.

Experimental

The Cu-Au alloyed nanoparticles with 10 at. % and 40 at. % Au were generated by vapor condensation method from a high purity Cu-Au ingot with purified helium in a vacuum chamber. The generated nano-particles were immediately carried with a helium flow through a stainless tube and deposited on an MgO (100) substrate (298 K) placed in another vacuum (specimen) chamber for grazing incident x-ray XRD measurements. Further details of the XRD performance have been described elsewhere [1]. The Au concentration of the prepared specimens was respectively estimated to be 10 and 40 at. % from the Cu-Au (111) Bragg angle which is very sensitive to the Cu-Au composition due to the large difference in radius between Cu and Au atom [2]. For the oxidation experiments, dry air was introduced into the XRD chamber with keeping a pressure at 9.3×10^{4} Pa and a substrate temperature at 298 K. During the oxidation, the XRD measurement was performed at 45 kV and 300 mA repeatedly once per hour until the intensity of the peaks showed practically no more change. After dry air exposing, the specimen was then rapidly transferred from the XRD chamber to XPS chamber via atmosphere air within 1 minute. The XPS measurement was performed in ultra-high vacuum (~10^{-9} Torr) and the accuracy of the electron analyzer is 0.1 eV. The Au $4f_{7/2}$ binding energy of high purity gold was used as an external standard. The deconvolution of the photoelectron peaks was fitted using XPSPEAK4.1 software. The Shirley background [3], and mixed Gaussian/ Lorentzian functions were used for the fitting. To see morphology and size distribution, Cu-Au nanoparticles were deposited on a holey carbon microgrid and transferred through air to a 200 kV transmission electron microscope (TEM), JEOL JEM-2010.

Results and discussion

Figure 1 shows the size distribution and the TEM micrograph of some deposited particles. The particles prepared by the present method frequently show icosahedral structure and have a size distribution from 5 to 36 nm with a volume-mean size of 20 nm. The particles stacked in a rather porous fashion. The Brunauer–Emmett–Teller (BET) surface area showed 15 m^2g^{-1}, indicating 55 % reduction from the isolated state.

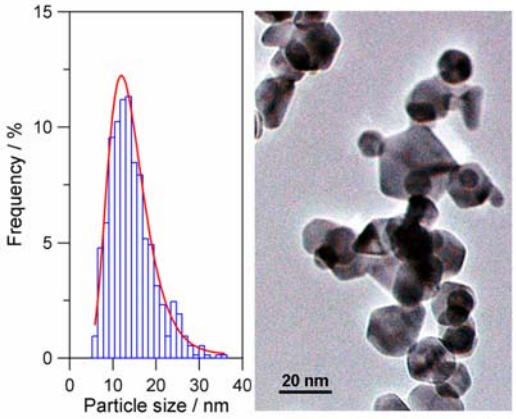

Fig.1. Size distribution and TEM image of Cu-40 at. % Au nanoparticles.

Figure 2 shows the x-ray diffraction patterns of (a) pure Cu, (b) Cu-10 at. % Au and (c) Cu-40 at. % Au nanoparticles before and after exposing to dry air. As can be seen, the XRD patterns of the as-deposited Cu and Cu-Au nanoparticles contain only a pair of diffracted peaks which correspond to Cu (111)/Cu(200) and Cu-Au(111)/Cu-Au(200), respectively. As well known, Cu has three typical oxides, i.e. Cu_2O, CuO and $Cu(OH)_2$. Depending on the experimental conditions, the surface oxide formed on Cu can consist of one or more species of the typical oxides. Our previous results [1] have indicated that Cu_2O is the only preferred oxide for the Cu nanoparticles as shown in Fig. 2(a). In Fig. 2(b), a broadening peak at 2θ =36.4^{o} can be indexed as the Cu_2O indicating the selective oxidation of the Cu component in the Cu-10 at. % Au particles. This selective oxidation will produce an Au-rich phase in the original Cu-Au alloy, so call the dealloying process. Since only little amount of Cu was oxidized

to Cu_2O, we cannot find significant Au-rich dealloyed phase from the XRD pattern in Fig. 2(b).

In the case of Cu-40 at. % Au particles, at the initial stage, the 111 and 200 peaks of Cu-Au showed a symmetric shape. As the air exposure time increased, these two peaks have been gradually asymmetric and broadened as shown in Fig. 2(c). Due to the high Au concentration, the Cu-Au(111) peak great shits to lower Bragg angle and overlaps with the oxide peaks as well as the dealloy peaks. It is thus of difficult to determine what kind of oxide it has from the XRD pattern.

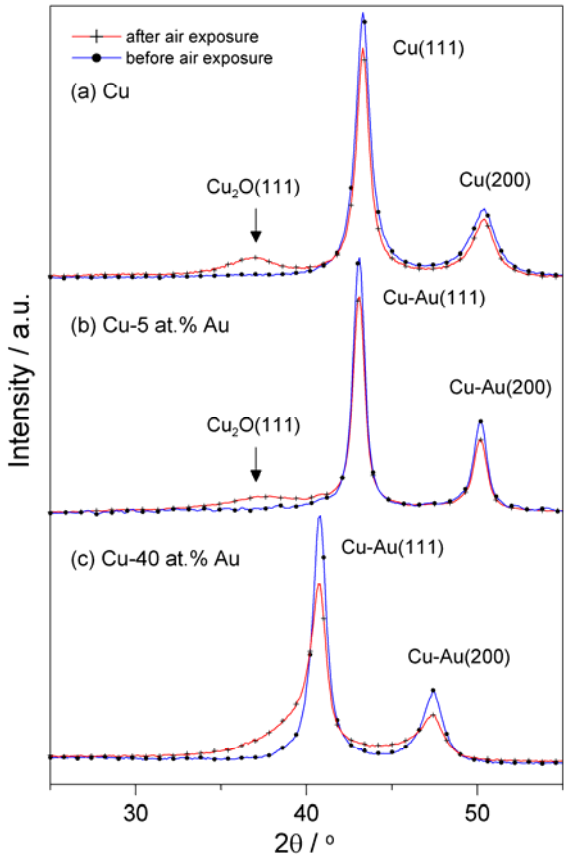

Fig. 2. In-situ x-ray diffraction patterns of (a) pure Cu, (b) Cu-10 at. % Au and (c) Cu-40 at. % Au nanoparticles before and after exposing to dry air for 100 hrs.

We analyzed the plot of intensity ratio versus time as can be seen in Fig. 3 in view of basic rate laws for the oxidation kinetics, i.e., logarithmic, inverse logarithmic, linear, parabolic, cubic and higher power rate laws [4]. At lower temperatures and in thin oxide films, the inverse-logarithmic equation based on the theory by Cabrera and Mott [5] has been often employed to explain oxidation kinetics of Cu bulk surfaces [4,6,7]. But, the

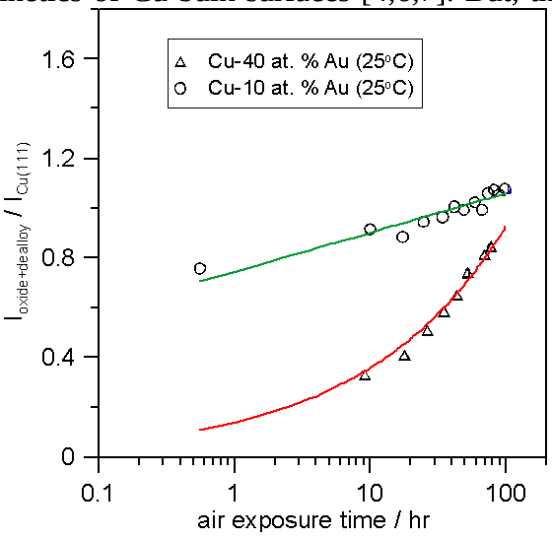

Fig. 3. The integrated intensity ratio obtained from XRD measurements versus the air exposure time at the pressure of 9.3×10^4 Pa on a linear-log scale for the 298 K data. The solid lines are drawn based on the data analysis results.

only equation to fit the data of Cu-10 at. % Au was found to be of direct-logarithmic, indicating the protective oxidation behavior. In contrast, Cu-40 at. % Au was described by cubic-like (n=2.5) oxidation law indicating the non-protective oxidation behavior.

Figure 4 shows XPS and Auger spectra of pure Cu, Cu-10 at. % Au and Cu-40 at. % nanoparticles. The XPS spectra of copper and its oxides, Cu_2O and CuO, and $Cu(OH)_2$, have been studied extensively. One can easily distinguish CuO and $Cu(OH)_2$ from metallic copper by a study of the $Cu2p_{3/2}$ peak because the binding energies of $Cu2p_{3/2}$ in CuO and $Cu(OH)_2$ are about 1.3±0.2 eV and 2.0±0.2 eV respectively higher than the that in metallic copper (932.5 eV). These two compounds can also be distinguished from the satellite peaks located at about 7.8 eV and 10.2 eV higher than the principal line of CuO and 6.2 eV and 9.0 eV of $Cu(OH)_2$ [8]. Due to a negligibly small chemical shift of about 0.1 eV, Cu_2O and metallic copper can not be distinguished from $Cu2p_{3/2}$ peak. However, the presence of Cu_2O can be identified by the Cu L_3VV Auger signal. The relative peak position of Cu and its oxides mentioned above were used for the XPS profile fitting as shown in Fig. 4. It can be easily seen that the oxide phase for Cu-10 at. % Au and for

Cu-40 at. % Au is Cu_2O and CuO, respectively. We can also find the presence of $Cu(OH)_2$ for both compositions. However, the comparable amount of $Cu(OH)_2$ shown in Fig. 4 cannot be observed in the XRD patterns in Fig. 2 indicates the existence of amorphous $Cu(OH)_2$.

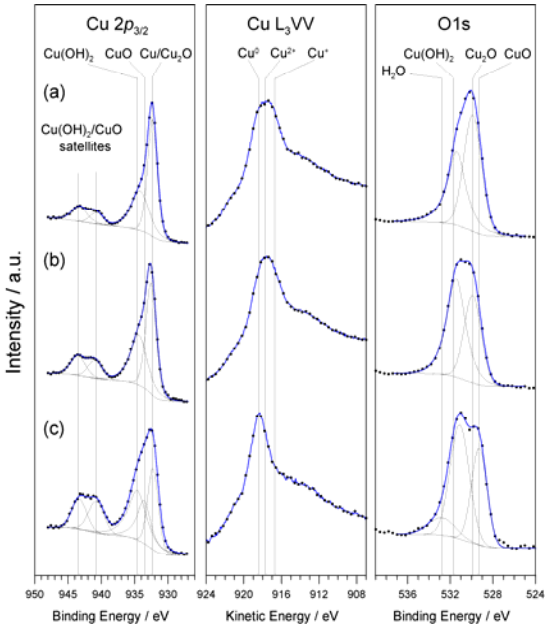

Fig. 4. XPS and Auger spectra of (a) pure Cu, (b) Cu-10 at. % Au and (c) Cu-40 at. % nanoparticles.

Conclusions

We have quantitatively observed the oxidation kinetics of Cu-Au nanoparticles and their compositional dependences. The oxidation behavior (protective or non-protective) was found to be directly related to the composition of Cu-Au nanoparticles. In addition, the XPS analysis showed the existence of Cu_2O and $Cu(OH)_2$ phases in the specimen of 10 at. % Au. Nevertheless, CuO and $Cu(OH)_2$ phases were the main oxides in the specimen of 40 at. % Au. The present result might provide a valuable data for basic understanding of the self-limiting oxidation kinetics of metal nanoparticles and also for control of their oxide thickness.

References

[1] K. Koga and H. Takeo, Rev. Sci. Instrum. 67, 4092, 1996; K. Koga, H. Takeo, T. Ikeda, and K. Ohshima, Phys. Rev. B 57, 4053, 1998.

[2] W. B. Pearson, A Handbook of Lattice Spacings Structure of Metals and Alloys, Pergamon Press, New York 1985.

[3] D. A. Shirley, Phys. Rev. B 5, 4709, 1972.

[4] A. Rönnquist, H. Fischmeister, J. Inst. Met. 89, 65, 1960-1961.

[5] N. Cabrera, N. F. Mott, Rep. Prog. Phys. 12, 163, 1948.

[6] K. Hauffe, Oxidation of Metals; Plenum Press: New York, 1965.

[7] A. T. Fromhold, Theory of Metal Oxidation; North-Holland: New York, 1976.

[8] N. S. Mclntyre, M. G. Cook, Analytical Chem. 47, 2208, 1975.